Ammonia at Blodgett Forest, Sierra Nevada, USA

Marc L. Fischer and David Littlejohn

Environmental Energy Technologies Division, E.O. Lawrence Berkeley National Laboratory,
1 Cyclotron Rd., Berkeley CA, 94720, USA

Corresponding author address:

Marc L. Fischer, Staff Scientist
Atmospheric Sciences Department
Mail Stop 90K-125
E.O. Lawrence Berkeley National Laboratory
1 Cyclotron Rd.
Berkeley, CA 94720-8108

Phone: 510-486-5539
email: mlfischer@lbl.gov

Abstract

Ammonia is a reactive trace gas that is emitted in large quantities by animal agriculture and other sources in California, which subsequently forms aerosol particulate matter, potentially affecting visibility, climate, and human health. We performed initial measurements of NH_3 at the Blodgett Forest Research Station (BFRS) during a two week study in June, 2006. The site is used for ongoing air quality research and is a relatively low-background site in the foothills of the Sierra Nevada. Measured NH_3 mixing ratios were quite low (< 1 to ~ 2 ppb), contrasting with typical conditions in many parts of the Central Valley. Eddy covariance measurements showed NH_3 fluxes that scaled with measured NH_3 mixing ratio and calculated aerodynamic deposition velocity, suggesting dry deposition is a significant loss mechanism for atmospheric NH_3 at BFRS. A simple model of NH_3 transport to the site supports the hypothesis that NH_3 is transported from the Valley to BFRS, but deposits on vegetation during the summer. Further work is necessary to determine whether the results obtained in this study can be generalized to other seasons.

1. Introduction

In California and the nation, many areas are out of compliance with federal particulate matter standards designed to protect human health (NRC 1998; NRC 2000). Nationally, Congress has set a goal to remediate current and prevent future impairment of visibility in over 150 federally designated Class 1 Federal (Malm et al. 2000) designated sites. Ammonia (NH_3) is the primary gas to form aerosols in combination with acidic species (e.g., SO_X, NO_X) that are produced in combustion processes from energy related activities. While mixing ratios of combustion derived species are regulated, NH_3 is not. If ammonia limits aerosol concentrations, then controls on emissions of NO_X and perhaps SO_X may not be effective in controlling aerosol concentrations, visibility, or protecting human health.

The magnitude of NH_3 fluxes are expected to vary enormously over space. NH_3 is emitted from strong point sources (e.g. animal agriculture), medium strength distributed sources (e.g., fertilized fields and automobile catalytic converters), and exchanged with spatially vast areas of soil and vegetation (Potter et al. 2001; Kirchstetter et al. 2002; Battye et al. 2003). Ammonia is of particular interest in California because it is emitted in large amounts from agricultural sources in the Central Valley, leading to high (20-40 ppb) surface layer NH_3 mixing ratios (Fischer et al. 2003; Lunden et al. 2003; Chow et al. 2006). For example, recent work suggest that San Joaquin Valley area emissions might range from 8 to 42 g N ha^{-1} day^{-1} (11 to 50 ng NH_3 m^{-2} s^{-1}) in winter and summer respectively, with approximately 78 % of the summertime emissions derived from animal agriculture (Battye et al. 2003).

While most NH_3 measurements have been made in urban areas in California, some measurements have been made in rural settings. Airborne measurements in the afternoon mixed layer showed that ammonium compounds (i.e., NH_3 + NH_4^+) were the dominant component of the N budget with variable NH_3 concentrations corresponding to mixing ratios of 10 ± 7 and 2.5 ± 0.5 ppb in boundary layer above the foothills of the Sierra in the boundary layer above Lake Tahoe respectively (Zhang et al. 2002). In contrast, a ground-based study at Lake Tahoe measured significantly lower concentrations corresponding to approximate mixing ratios

between 0.6 to 1.5 ppb and mean summer deposition rates between 3 to 11 ng N m^{-2} s^{-1} (Tarnay et al. 2001). The previous work raises the question of whether there are vertical gradients in NH_3 caused by dry deposition or whether the differences in NH_3 at the surface and aloft are due to different measurement times.

Here we describe a short term study of the NH_3 mixing ratios and NH_3 fluxes at a rural site in the foothills of the Sierra Nevada.

2. Methods

The methods section includes a description of the measurement site, the fast response NH_3 instrument, the methods used for data reduction, a filter sampling system used to provide comparative NH_3 measurements, a method used to calculate the aerodynamic deposition velocity expected under different meteorological conditions, and a predictive model for NH_3 mixing ratios at the measurement site.

2.1 Measurement Site

UC Berkeley Blodgett Forest Research Station

We measured NH_3 mixing ratios and fluxes near the University of California's Sierra Nevada the Blodgett Forest Research Station (BFRS), located west of the Sacramento region as shown in Figure 1. The BFRS site is an attractive site for this work because it is representative of large areas of forested land with acidic soils in the mountainous Western US and has been the site of ongoing air quality measurements (Goldstein et al. 2000; Dillon et al. 2002; Kurpius et al. 2002; Farmer et al. 2006). Although recent work at BFRS has studied mixing ratios and fluxes of several reactive nitrogen species, NH_3 has not been measured previously.

The BFRS tower is located at 38.88°N, 120.62°W, at an elevation of 1315 m in a re-growing ponderosa pine plantation. Tree heights ranged from approximately 8-10 m. Terrain is gently sloping downward from east to west. Power to the site is provided by a diesel generator located approximately 130 m due north of the tower site. The predominant winds are upslope from the southwest during the day and downslope from the northeast during the night.

2.2 *NH_3 Instrument*

Ammonia was measured using a sensitive fast-response quantum-cascade laser (QCL) spectrometer operating at a frequency of 965 cm^{-1} (Aerodyne Research Inc (ARI), similar to that used for eddy covariance flux measurements of NO_2 (Zahniser 2003; Horii et al. 2004). The precision of the NH_3 instrument is normally 0.3 ppb (1 sigma) for data collected at a frequency of 10 Hz. The instrument provided highly automated control of high frequency data collection, zero adjustments, and zero and span checks as described below using a dedicated software package (TDLWintel).

In addition to the QCL spectrometer, additional data was collected. First, a sonic anemometer (Gill Windmaster Pro) was used to measure fluctuations in virtual air temperature and 3-D winds. The digital output from the anemometer was logged by the computer controlling the QCL spectrometer. The anemometer was physically positioned so that the sensing volume was located 30 cm from the inlet manifold of the NH_3 instrument. Second, a data logger (Campbell CR23X) recorded gas flow rates controlled by mass flow controllers, inlet surface temperatures measured with thermocouples, atmospheric temperature and relative humidity (Vaisala Y45), and short wave solar radiation (Kipp and Zonen CM3).

The NH_3 and ancillary meteorological measurements were made at a height of approximately 10 m above the ground, sufficient to reach slightly above the nearby vegetation. The combined weight of the spectrometer, support electronics and thermal control system and liquid nitrogen storage dewar for automated refills of the spectrometer detector dewar (total of ~ 200kg) required a platform scissor-lift. The scissor lift was located at a distance of approximately 8 m from the main BFRS meteorological tower. During the two day period from July 24 to 25, when the LBNL measurements were compared with the filter sampler, the platform was lowered to a height of ~ 6 m to match the height of the filter sampler. The filter sampler was deployed on the main BFRS tower.

To achieve high temporal resolution necessary for eddy covariance measurements, we designed a high flow rate gas sampling and calibration subsystem that transmits ambient NH_3 vapor to the spectrometer with minimal residence time. A schematic of the inlet and calibration system is

shown in Fig. 2. A flow of ambient air is drawn into the sample manifold by the combination of a manifold flow pump (at 20 slpm) and into the NH_3 spectrometer at a rate (approximately 25 slpm) determined by the pump speed (Varian 600 dry scroll) and the diameter of a critical orifice inlet. After entering the critical orifice (which reduces the pressure to approximately 50 Torr), air is passed through a 0.2 micron PTFE air filter (Gelman PALL, Acro-50), a 2 m long 1 cm diameter PFA Teflon tube to the multipass optical cell contained within the QCL spectrometer. All glass surfaces are siloxyl coated (General Electric) and surfaces are heated as suggested in Neuman et al (1999). In our application, the temperatures of the different inlet parts were maintained between 40 and 45°C by a set of four temperature control circuits, while the optical bench including the optical absorption cell was maintained at 30°C.

During the measurements, the instrument zero was adjusted every 30 minutes, under control of the spectrometer computer, by overfilling the inlet manifold with an approximately 60 slpm flow of dry nitrogen supplied by a large liquid N_2 supply dewar. Typically, zero adjustments were significantly less than 1 ppb. In addition, the instrument zero and span were checked periodically. Zeros were generally checked every 30 minutes. The span of the instrument was checked by reversing a backflow of 300 sccm that normally removes a 100 sccm flow of NH_3 supplied from a permeation tube source. After applying NH_3 for 30 s, the backflow is reestablished removing NH_3 from the inlet. The response time of the instrument to an approximately 15 ppb step in NH_3 mixing ratio was checked once each hour by applying a NH_3 from a permeation tube source to the N_2 flow. As shown in Figure 3, the response is well characterized by the sum of exponential decay terms as

$$NH_3(t) = No\,(a_1 \exp(-t/\tau_1) + a_2 \exp(-t/\tau_2)), \quad (1)$$

where a1 = 0.8 +/- 0.05, τ_1 = 0.35 +/- 0.05 s, $a_2 = (1-a_1)$, and τ_2 = 4 +/- 1 s. The uncertainties in the values reported for the decay coefficients time constants represent variations in the best fit values obtained from fits taken over the experimental period.

2.3 Data Reduction

The 10Hz data NH_3 were processed to estimate mean NH_3 mixing ratios and NH_3 fluxes. For mean NH_3, a continuous estimate of instrument zero was estimated as a spline interpolation of

NH_3 values obtained during the stable period at the end of zero checks (see Figure 3). The instrument zero was less than 1 ppb for 90% of the data, until June 21st, when the instrument ran out of cryogens. Upon restarting the instrument on June 23rd, the instrument noise level had increased by nearly an order of magnitude (to ~ 3 ppb in 1 second integration), leading to a larger variation in zero level. Following subtraction of instrument zeros, mean mixing ratios were calculated for 1 and 12 hour bins.

NH_3 flux was computed for ½ hour intervals from the covariance of the 10 Hz NH_3 mixing ratios and the vertical wind using standard techniques (Baldocchi et al. 1988). Wind fields were rotated to a coordinate system with zero mean vertical wind. Fluctuations in ammonia, NH_3', virtual temperature, T', and wind vectors, u', v', and w', were calculated by subtracting 1/2 hour block averages. Vertical fluxes were calculated as the covariance between vertical wind fluctuations, w', and other quantities. Periods during NH_3 zero or span measurements were excluded. The mean ammonia flux, $F_{NH3} = \langle w'NH_3' \rangle$ was estimated for each ½ hour interval. The time lag between w' and NH_3', required to maximize F_{NH3}, was determined from lag correlation plots. Typical values for the best lag were small (< 0.3 s), and roughly consistent with that expected from the measured step response of the inlet system.

To correct for loss of high frequency NH_3 fluctuations due to finite frequency response of the gas inlet, we applied an empirically derived multiplicative correction (Horii et al. 2004). The correction was computed from the measurements of sensible heat obtained from the sonic anemometer. Here sensible heat is calculated as, $H = \rho C_p \langle w'T' \rangle$, where ρ and C_p are the density and specific heat of air respectively. We calculated the correction factor,

$$f_{corr} = w'T' / w'T_{sm}', \qquad (2)$$

where T_{sm}', is obtained by convolving T' with the double exponential decay function describing the step response to NH_3 span decay in Eq (1). Typical values for F_{corr} ranged from 1 to 1.2 depending on the atmospheric stability, indicating that the NH_3 captured most of the high frequency fluctuations contributing to the flux. As an additional check of the frequency response, power spectra for w'T', $w'T_{sm}$', and $w'NH_3$' were computed for ½ hour periods and compared with the -4/3 power law expected from Komolgorov similarity theory.

We determined whether the NH_3 fluxes were stationary by comparing the ½ hour mean flux with the mean of the individual fluxes determined from 5 minute sub-intervals. Data was considered to be stationary when the flux calculated from the subintervals is within 30% of the ½ hour mean flux (Foken et al. 1996). Non-stationary conditions typically occur during periods of intermittent turbulence which typically occurs on nights when the air is stably stratified and friction velocity, $u^* = <-w'u'>^{1/2}$ is low ($u^* < 0.1$ m s^{-1}). Non-stationary fluxes of nitrogen oxides have also been observed at BFRS, associated with emissions from the generator (Farmer et al. 2006). We excluded the data (~ 20%) obtained when the wind direction was within 45 degrees of north.

2.4 Filter Sampling

Ambient NH_3 concentrations were determined during a two day period (starting on the evening of June 23rd and continuing into midday of June 25th) using filter samples collected with the Desert Research Institutes (DRI) sampler (Chow et al. 1993). As described above, the inlet of the filter sampler was located at a height of 5.5 m off the ground on the main meteorological tower. In this method, two filter samples are collected simultaneously. One filter is exposed to a flow of ambient air, while the other is exposed to air that has had gaseous NH_3 removed by an annular denuder. Then the denuded filters collected only particulate NH_4^+, while the undenuded filter collected both gas and aerosol. Gaseous NH_3 is estimated as the difference between undenuded and denuded measurements. In this experiment, four sets of paired (denuded and undenuded) citric acid coated filters were exposed to air flows near 100 liters per minute (measured before and after each sample was collected) over the two day period using 12 hour collection times (1800-0600 and 0600-1800 PDT, or 0100-1300 and 1300-0100 GMT). Before and after sample collection the filters were stored in capped, bagged, and stored in an ice chest. Following collection on June, 25th, the samples were returned to DRI for analysis of NH_4^+ ions captured on the citric acid.

2.5 Estimate of Maximum Deposition Velocity

As a check on the observed NH_3 fluxes, we computed deposition velocities, $V_d = F_{NH3}/NH_3$, for each ½ hour interval and compared it to a simple model for the maximum deposition velocity expected if all NH_3 molecules are reaching the leaf surfaces are adsorbed. In general, deposition velocity can be expressed in a resistance based model as,

$$V_d = (R_a + R_b + R_c)^{-1}, \quad (3)$$

where R_a, R_b, and R_c, are the aerodynamic, leaf boundary layer, and stomatal resistances respectively. In the limit that the vegetation is nitrogen limited and readily accepts all NH_3 reaching the leaf surface, R_c can be assumed to be small and a maximum deposition velocity can be written as

$$V_{dmax} = (R_a + R_b)^{-1}, \quad (4)$$

Using standard turbulence models for the surface layer fluxes, one can write a set of expressions for R_a and R_b (Wesely 1989; Horii et al. 2004). Here

$$R_a = u/u^{*2} - \chi_H/(ku^*), \quad (5)$$

where k is the Von Karmen coefficient (~ 0.4). Under stable conditions χ_H can be expressed as

$$\chi_H = 5(z-d)/L, \quad (6)$$

where z is the measurement height, d is the displacement height (often assumed to be 0.75 vegetation height), and L is the Monin–Obukhov length scale, $L = -kg\langle w'T'\rangle/Tu^{*3}$, and g is the acceleration due to Earth's gravity. Stable conditions are defined as when $L > 0$. Under unstable conditions ($L < 0$),

$$\chi_H = \exp(0.598 + 0.39 * \ln(-(z-d)/L) - 0.09 * (\ln(-(z-d)/L))^2). \quad (7)$$

Finally, the boundary layer resistance at the leaf surface can be written as

$$R_b^{-1} \sim u^*/7.1 \quad (8)$$

Under the conditions observed at a mixed deciduous forest in Northeastern United States, Horri et al. (2004) observed $0.01 < V_d < 0.08$ m s^{-1}.

2.6 Simulation of NH_3 Mixing Ratios

Measured NH_3 mixing ratios were compared with simulated NH_3 concentrations derived from and a regional emission inventory estimate of NH_3 emissions combined with a particle back trajectory calculation of time and space specific surface influence on atmospheric gas concentrations and dry deposition of NH_3.

A simple NH_3 emission model was used for these simulations. NH_3 emissions for June were estimated assuming that cows in dairies and feedlots generated a large fraction of the emissions in the Central Valley. The spatial distribution of cows was obtained from county level statistics for 2002 animal stocking density reported by the United States Department of Agriculture's

National Agricultural Statistics Service (NASS, 2004). We estimated the NH_3 emission factors for the summer conditions by scaling the annual averaged emissions factors by the ratio (2.3) of summer time animal fluxes to annually averaged animal fluxes in the San Joaquin Valley (Battye *et al.* , 2003). The resulting emissions factors are 185 and 64 g NH_3 animal^{-1} day^{-1} for dairy and non-dairy cattle respectively. County level NH_3 fluxes were calculated as the total NH_3 emissions for each county normalized by the area and are shown in Table 1. Fluxes from Nevada were set equal to the 2 ng m^{-2} s^{-1}, similar to low emission counties in California. We did not attempt to include other sources of NH_3 emission (e.g, other animal agriculture or automobiles) and hence this estimate likely represents a lower limit to NH_3 fluxes. However, we consider this simple model roughly sufficient for determining the temporal variations in NH_3 expected at BFRS, particularly given the additional approximations we make in estimating the transport of NH_3 from remote locations to the site.

The surface influence functions were calculated using the stochastic time inverted Lagrangian transport (STILT) model (Lin et al. 2003). STILT was originally derived from the NOAA HYSPLIT particle transport model (Draxler et al. 1998) for inverse model estimates of surface CO_2 fluxes (Lin et al. 2004). In our simulations, ensembles of 100 particles were released from the tower site every 2 hours and run backward in time for a period of 12 hours, which generally allowed the particles to reach locations in the central valley. STILT was driven with NOAA reanalysis meteorology (EDAS40) with 40 km spatial resolution and hourly temporal resolution. Land surface contributions to atmospheric NH_3 were assumed to be proportional to the time a particle spends within the surface boundary layer. NH_3 deposition was assumed to depend on the rate of vertical mixing in the atmosphere and parameterized as a residence time $\tau = z / V_{d0}$, where z is the particle altitude above ground and $V_{d0} = 0.02$ m s^{-1} is an assumed mean deposition velocity. For each time step, Δt, NH_3 is updated as

$$NH_3 (t + \Delta t) = NH_3 (t)\, e^{-\Delta t/\tau} + F_{NH3}\, \Delta t / z_i\, \nu, \qquad (8)$$

where F_{NH3} (nmol m^{-2} s^{-1}) is the surface NH_3 flux at the position of the particle, z_i is the height of the boundary layer, and ν is the molecular density of air. Simulations were run both with and without the deposition loss term to estimate the concentration expected for a non-reacting gas.

3. Results and Discussion

3.1 Surface NH_3 Mixing ratios

Figure 4 shows the hourly averages of measured NH_3 from the LBNL laser spectrometer and the mean results from the 12 hour samples collected by the DRI filter system. Both LBNL and DRI data show that NH_3 was generally between 0 and 2 ppb, with a few periods of higher mixing ratios. Near June 13th, a synoptic event introduced cooler air from the north with lower temperatures and mild precipitation, reducing NH_3 concentrations significantly. The averages of the LBNL measurements were lower than the filter samples on June 24th, and similar to or higher than the filter samples on June, 25th (see Table 2). Inspection of the LBNL data suggests that a significant fraction of the data was noisy and did not pass quality control criteria (~ 50% in some of the 12 hour periods), perhaps causing the poor correlation between LBNL averages and the DRI filter measurements.

We also examined the diurnal variations in NH_3. As shown in Figure 5, there was a significant diurnal cycle with lower mixing ratios at night and higher mixing ratios during the day. This is consistent with having predominantly downslope winds carrying NH_3 free air from the Sierra Nevada during the night and upslope winds carrying air with NH_3 from the Central Valley during the day (Dillon et al. 2002).

3.2 Calculated Aerosol – Gas Equilibrium

We considered whether the low NH_3 mixing ratios might limit ammonium-based aerosol concentrations by comparing measured NH_3 with previously measured HNO_3 and the aerosol-gas equilibrium coefficient, Kp, which defines the minimum NH_3*HNO_3 product required to form NH_4NO_3 aerosol (Stelson et al. 1982). Figure 6 shows that Kp >> 1 ppb^2 for most of the observation period. Earlier work at Blodgett showed that HNO_3 mixing ratios fell in a range of 0.3 to 1.5 ppb (5%-95%) for June-October (Murphy et al., 2006). Assuming a nominal value of 1 ppb HNO_3, the minimum NH_3 mixing ratio required to support aerosol NH_3*HNO_3 in equilibrium with gas phase constituents is numerically equal to the value of Kp. Since the measured NH_3 mixing ratio is generally significantly less than Kp, this suggests that aerosol NH_3*HNO_3 will not be present in equilibrium with gases. We also note that although Kp was

low during points earlier in June, there were also light rains, which would likely strip NH_3, HNO_3, and aerosols from ambient air.

3.3 NH_3 Fluctuations, Fluxes, and Deposition Velocities

Before computing NH_3 fluxes, we examined the power spectra for temporal variations in w'T', w'T'$_{sm}$, and w'NH_3 for each ½ hour period over which NH_3 fluxes were calculated. By comparing the spectra of w'T' and w'T'$_{sm}$, we can visually inspect the loss of high frequency power in w'T' introduced by smoothing T' with the finite frequency response of the NH_3 inlet system. A representative set of power spectra are shown in Figure 7. As expected, the spectra for w'T' and w'T'$_{sm}$ are similar, consistent with the smoothing reducing w'T' by a small amount, and suggesting that NH_3 fluxes can be accurately recovered. We also note parenthetically that the high frequency slope of all three of the spectra was not as steep as that expected for turbulence in a Komolgorov similarity theory, as observed by other researchers at this and other sites (Farmer et al. 2006).

The NH_3 fluxes calculated from the 10Hz data are shown in Figure 8. Most of the NH_3 fluxes were small (~ 10 ng NH_3 m^{-2} s^{-1}) or negative. During a several day period early in the campaign when NH_3 mixing ratios were highest, large negative fluxes (- 30 ng NH_3 m^{-2} s^{-1}) were observed, indicating that NH_3 was being lost to the canopy by dry deposition. The mean flux during the measurement period was 9.2 ± 1.1 ng NH_3 m^{-2} s^{-1}. As a check of whether the estimated fluxes were realistic, we calculated deposition velocities for a subset of the measured fluxes. The subset was obtained by requiring that the NH_3 mixing was known to better than 50% (at 68% confidence). As shown in Figure 9, the measured deposition velocities are all less than the maximum deposition velocity estimated from the measured turbulence conditions using Eq (8), with a typical ratio for the measured to maximum deposition velocity of approximately 0.5. This is consistent with some combination of imperfect sticking to leaf surfaces and stomatal resistance to NH_3 uptake by the leaves.

3.4 Transport Model Estimates of NH_3 Concentrations

The map of the estimated surface NH_3 fluxes from cattle is shown in Figure 10. Surface fluxes range over several orders of magnitude, reflecting the strong emissions from the Central Valley and low emissions from the mountainous regions of the Sierra Nevada. Figure 10 includes an

example ensemble of 12-hour particle back-trajectories representing a measurement at BFRS at 1300 hours local time on June 12th, 2006. This example shows that some particle tracks sweep backward into the Central Valley where they come into contact with high surface NH_3 fluxes.

The predicted NH_3 concentrations from the back trajectory simulations are compared with measured NH_3 in Figure 11. Measured NH_3 is generally a factor of ~ 2 higher than NH_3 predicted with deposition and a factor of ~ 2 less than NH_3 predicted without deposition. The temporal variations in predicted and measured NH_3 mixing ratios match reasonably well. This is likely because the large variations are caused by variations in the amount of air reaching BFRS from areas in the Central Valley where NH_3 fluxes are highest.

4. Conclusions

We performed an exploratory study of NH_3 mixing ratios and fluxes at Blodgett Forest during June, 2006. The 1 hour averaged NH_3 mixing ratios ranged from non-detection (< 0.2 ppb) to about 2 ppb, typical of a low-background site removed from significant sources. The diurnal variations were consistent with upslope flows bringing air with higher NH_3 to the site during the day. The observed NH_3 mixing ratios were not sufficient to support NH_4NO_3 aerosol in equilibrium with gas phase NH_3 assuming HNO_3 was similar to that observed at the site previously. NH_3 fluxes, measured using the eddy covariance method, were generally small or negative, consistent dry deposition to the vegetation and no significant net emission. Calculated deposition velocities were generally about half of the maximum expected for deposition to a canopy with aerodynamic and leaf boundary layer resistance but no resistance to leaf uptake (perfect sticking to leaves). This is not surprising given the nitrogen poor soils in the Sierra foothills. Last, we predicted NH_3 at BFRS by combining a simple NH_3 emission inventory that considered only emissions from cows (dairy and meat) with a particle back-trajectory model. Measured and predicted NH_3 concentrations showed substantially similar temporal patterns over synoptic time periods. Predictions with and without NH_3 deposition bracketed the measured NH_3 mixing ratios. On the basis of these measurements, we conclude that NH_3 from the Central Valley had a small but measurable effect on NH_3 mixing ratios at the BFRS site during the short period of this study, but further measurements would be necessary to determine the whether the same patterns prevail over longer periods, particularly between different seasons.

Acknowledgements

We acknowledge Benet Duncan, Dennis Dibartolomeo, and Joshua Hatch for assistance in construction of the instrument packaging and thermal control systems, Mark Zahniser and David Nelson for technical advice on the use of the NH_3 spectrometer. Allen Goldstein generously shared the research infrastructure at BFRS, while David and Sheryl Rambeau provided invaluable assistance with arrangements for field work at BFRS. Steven Kohl of the Desert Research Institute prepared the filter sampler and performed the analysis of the integrated NH_3 mixing ratios. John Lin generously provided the STILT model for the atmospheric transport simulations. The NOAA Air Resources Laboratory (ARL) provided the assimilated meteorology used to drive STILT. Nancy Brown, Ron Cohen, Delphine Farmer, Martin Gallagher, Ash Lashgari, Melissa Lunden and Tom Ryerson provided valuable advice and discussion. This work was supported by the California Air Resources Board and by the Laboratory Directors Research and Development Program at the Lawrence Berkeley National Laboratory.

6. References

Baldocchi, D. D., B. B. Hicks and T. P. Meyers (1988). Measuring Biosphere-Atmosphere Exchanges of Biologically Related Gases with Micrometeorological Methods. Ecology (Tempe) **69**(5): 1331-1340.

Battye, W., V. P. Aneja and P. A. Roelle (2003). Evaluation and improvement of ammonia emissions inventories. Atmospheric Environment **37**(27): 3873-3883.

Chow, J. C., L. W. A. Chen, J. G. Watson, D. H. Lowenthal, K. A. Magliano, K. Turkiewicz and D. E. Lehrman (2006). PM2.5 chemical composition and spatiotemporal variability during the California Regional PM10/PM2.5 Air Quality Study (CRPAQS). Journal of Geophysical Research-Atmospheres **111**(D10).

Chow, J. C., J. G. Watson, J. L. Bowen, C. A. Frazier, A. W. Gertler, K. K. and D. L. Fung, and L. L. Ashbaugh (1993). A sampling system for reactive species in the western United States. Sampling and Analysis of Airborne Pollutants. E. D. Winegar and L. H. Keith. New York, A.F. Lewis**:** 209–228.

Dillon, M. B., M. S. Lamanna, G. W. Schade, A. H. Goldstein and R. C. Cohen (2002). Chemical evolution of the Sacramento urban plume: Transport and oxidation - art. no. 4045. Journal of Geophysical Research-Atmospheres **107**(D5-D6): 4045.

Draxler, R. R. and G. D. Hess (1998). An overview of the HYSPLIT_4 modeling system for trajectories, dispersion, and deposition. Australian Meteorological Magazine **47**: 295-308.

Farmer, D. K., P. J. Wooldridge and R. C. Cohen (2006). Application of thermal-dissociation laser induced fluorescence (TD-LIF) to measurement of HNO3, Sigma alkyl nitrates, Sigma peroxy nitrates, and NO2 fluxes using eddy covariance. Atmospheric Chemistry and Physics **6**: 3471-3486.

Fischer, M. L., D. Littlejohn, M. M. Lunden and N. J. Brown (2003). Automated measurements of ammonia and nitric acid in indoor and outdoor air. Environmental Science & Technology **37**(10): 2114-2119.

Foken, T. and B. Wichura (1996). Tools for quality assessment of surface-based flux measurements. Agricultural and Forest Meteorology **78**(1-2): 83-105.

Goldstein, A. H., N. E. Hultman, J. M. Fracheboud, M. R. Bauer, J. A. Panek, M. Xu, Y. Qi, A. B. Guenther and W. Baugh (2000). Effects of climate variability on the carbon dioxide, water, and sensible heat fluxes above a ponderosa pine plantation in the Sierra Nevada (CA). Agricultural & Forest Meteorology **101**(2-3): 113-129.

Horii, C. V., J. W. Munger, S. C. Wofsy, M. Zahniser, D. Nelson and J. B. McManus (2004). Fluxes of nitrogen oxides over a temperate deciduous forest. Journal of Geophysical Research-Atmospheres **109**(D8).

Kirchstetter, T. W., C. R. Maser and N. J. Brown (2002). Ammonia emisson inventory for the state of Wyoming. Berkeley, CA, E.O. Lawrence Berkeley National Laboratory.

Kurpius, M. R., M. McKay and A. H. Goldstein (2002). Annual ozone deposition to a Sierra Nevada ponderosa pine plantation. Atmospheric Environment **36**(28): 4503-4515.

Lin, J. C., C. Gerbig, S. C. Wofsy, A. E. Andrews, B. C. Daube, and B. B. S. C. A. Grainger, P. S. Bakwin, and D. Y. Hollinger (2004). Measuring Fluxes of Trace Gases at Regional Scales by Lagrangian Observations:

Application to the CO2 Budget and Rectification Airborne (COBRA) Study. J. Geophys. Res. **109**: doi:10.1029/2004JD004754, 2004.

Lin, J. C., C. Gerbig, S. C. Wofsy, A. E. Andrews, B. C. Daube, K. J. Davis and C. A. Grainger (2003). A near-field tool for simulating the upstream influence of atmospheric observations: The Stochastic Time-Inverted Lagrangian Transport (STILT) model - art. no. 4493. Journal of Geophysical Research-Atmospheres **108**(D16): 4493.

Lunden, M. M., K. L. Revzan, M. L. F. L. Thatcher, D. Littlejohn, S. V. Hering and N. J. Brown (2003). The transformation of outdoor ammonium nitrate aerosols in the indoor environment. Atmospheric Environment **37**: 5633-5644.

Malm, W. C., M. L. Pitchford, M. Scruggs, J. F. Sisler, R. Ames, S. Copeland, K. A. Gebhart and D. E. Day (2000). Spatial and Seasonal Patterns and Temporal Variability of Haze and It's Constituents in the United States. Fort Collins, Cooperative Institute for Research in the Atmosphere, Colorado State University.

Murphy, J. G., A. Day, P. A. Cleary, P. J. Wooldridge and R. C. Cohen (2006). Observations of the diurnal and seasonal trends in nitrogen oxides in the western Sierra Nevada. Atmospheric Chemistry and Physics 6: 5321-5338.

NRC (1998). Research priorities for airborne particulate matter. I. Immediate priorities and a long-range research portfolio. Washington, DC, National Academy Press.

NRC (2000). Research priorities for airborne particulate matter. III. Early Research Progress. Washington, DC, National Academy Press.

Potter, C., C. Krauter and S. Klooster (2001). Statewide Inventory Estimates Statewide Inventory Estimates of Ammonia Emissions from of Ammonia Emissions from Native Soils and Chemical Native Soils and Chemical Fertilizers in Fertilizers in California. Sacramento, California Air Resources Board.

Stelson, A. W. and J. H. Seinfeld (1982). Relative-Humidity and Temperature-Dependence of the Ammonium-Nitrate Dissociation-Constant. Atmospheric Environment **16**(5): 983-992.

Tarnay, L., A. W. Gertler, R. R. Blank and G. E. Taylor (2001). Preliminary measurements of summer nitric acid and ammonia concentrations in the Lake Tahoe Basin air-shed: implications for dry deposition of atmospheric nitrogen. Environmental Pollution **113**(2): 145-153.

Wesely, M. L. (1989). Parameterization of Surface Resistances to Gaseous Dry Deposition in Regional-Scale Numerical-Models. Atmospheric Environment **23**(6): 1293-1304.

Zahniser, M. S. (2003). Urban Ammonia Source Characterization Using Infrared Quantum Cascade Laser Spectroscopy. National Atmospheric Deposition Program (NADP) Meeting, Potomac, MD.

Zhang, Q., J. J. Carroll, A. J. Dixon and C. Anastasio (2002). Aircraft measurements of nitrogen and phosphorus in and around the Lake Tahoe Basin: Implications for possible sources of atmospheric pollutants to Lake Tahoe. Environmental Science & Technology **36**(23): 4981-4989.

455

456 ## 7. Tables

457 Table 1. Cattle stocking, area, and estimated NH_3 flux by county.

County	Beef Cows	Dairy Cows	Other Cattle	area (km^2)	Flux (ng NH_3 m^{-2} s^{-1})
Alameda	9401	6	10405	1888	8
Alpine	1560	0	551	1891	1
Amador	10112	20	9104	1518	9
Butte	8979	1261	9191	4197	4
Calaveras	14390	222	12878	2611	8
Colusa	0	0	7957	2946	2
Contra Costa	0	0	11596	1843	5
Del Norte	1018	4703	4154	2580	5
El Dorado	4115	9	3551	4380	1
Fresno	23422	90550	282547	15265	28
Glenn	17438	17304	30655	3366	22
Humboldt	22333	16732	24041	9146	8
Imperial	0	0	386634	10687	27
Inyo	0	0	8278	26120	0
Kern	36779	74708	148553	20841	14
Kings	5130	138292	126108	3561	111
Lake	4764	4	4378	3220	2
Lassen	25381	38	23905	11667	3
Los Angeles	0	0	2092	10396	0
Madera	15723	48086	82972	5468	32
Marin	9105	10309	15998	1331	31
Mariposa	10204	245	12130	3715	5
Mendocino	0	0	7691	8983	1
Merced	29534	223303	212270	4937	133
Modoc	41564	14	33615	10097	6
Mono	2989	0	2938	7794	1
Monterey	25430	1606	46025	8504	7
Napa	4300	245	3453	1930	3
Nevada	3007	108	1927	2451	2
Orange	392	0	401	2021	0
Placer	0	0	10004	3595	2
Plumas	5766	7	10644	6537	2
Riverside	3670	90359	87042	18451	14
Sacramento	16392	18337	32807	2472	31
San Benito	14408	935	24054	3556	9
San Bernardino	2918	158240	110185	51334	8
San Diego	6363	5729	13709	10752	3
San Francisco	0	0	0	120	0

San Joaquin	19629	103534	95196	3582	86
San Luis Obispo	38268	550	44928	8459	7
San Mateo	1474	6	941	1150	2
Santa Barbara	19482	2669	21183	7007	5
Santa Clara	0	0	12692	3304	3
Santa Cruz	984	176	2275	1140	2
Shasta	16618	562	11225	9690	2
Sierra	3339	0	3777	2441	2
Siskiyou	34750	1518	28421	16094	3
Solano	14560	3947	26605	2123	18
Sonoma	14311	31986	35301	4034	26
Stanislaus	42007	162878	221060	3824	142
Sutter	0	0	5321	1543	3
Tehama	29027	5489	33679	7555	8
Trinity	2671	12	2252	8137	0
Tulare	31171	412462	456491	12349	101
Tuolumne	6855	108	5288	5723	2
Ventura	4357	17	4544	4724	1
Yolo	6773	2012	8124	2594	6
Yuba	7419	3325	20694	1615	17

458

459 Table 2. Comparison of NH_3 mixing ratios (ppb) from DRI filter samples and averages

Date time (GMT)	Filter		LBNL	
24/06/2006 7:00	1.46	(0.05)	0.74	(0.28)
24/06/2006 19:00	1.55	(0.05)	0.36	(0.13)
25/06/2006 7:00	0.90	(0.12)	0.56	(0.32)
25/06/2006 19:00	0.58	(0.14)	0.91	(0.30)

8. Figure Captions

Fig 1. Satellite mosiac image showing the Blodgett Forest Research Station in the forested western foothills of the central Sierra Nevada of California, and the mixed use (agricultural and urban) areas of the nearby Sacramento Valley area.

Fig 2. Schematic illustration of the air sampling manifold with critical orifice flow inlet and air filter. Automated instrument zero and span calibrations are performed by periodically flowing N_2 into inlet, either without or with the addition of NH_3 from a permeation tube source.

Fig 3. Time series of NH_3 mixing ratio showing transient decay following removal of NH_3 span gas from zero air flow to instrument inlet.

Fig 4. Hourly NH_3 mixing ratios measured at Blodgett Forest in June, 2006. NH_3 data from the laser-spectrometer (black symbols) are averaged into 12 hour bins for comparison with integrating filter samples (blue symbols) collected with a sampling system provided by the Desert Research Institute.

Fig 5. Mean diurnal variation in surface NH_3 mixing ratio from June 11th to 26th, 2006.

Fig 6. Comparison of NH_3 mixing ratio (black) and aerosol-gas equilibrium partitioning coefficient, Kp (red), indicating minimum product of gas phase NH_3 and HNO_3 mixing ratios necessary for NH_4NO_3 aerosol to be found in equilibrium with gas phase constituents.

Figure 7. Power spectra of covariance in vertical wind speed with sonic temperature, w' T' , smoothed sonic temperature, w' T' $_{sm}$, and fluctuations in NH_3 mixing ratio, w' NH_3' . The straight line in upper right shows -4/3 slope expected for fluctuation spectra in an inertial sublayer.

Figure 8. Eddy covariance measurement of NH_3 flux for all time points (crosses) and for those passing quality control criteria for use in calculating deposition velocities (filled squares).

Figure 9. Scatter plot comparison of measured deposition velocity, v_d, and maximum deposition velocity in the case that all molecules reaching the leaf surface are absorbed, v_{dmax}.

Figure 10. Figure 10. Map of California showing estimated NH_3 emissions (ng NH_3 m^{-2} s^{-1}) and an example 12hr back trajectory calculation of showing particles converging at BFRS at midday on June 12th, 2006.

Figure 11. Measured hourly NH_3 mixing ratios from LBNL system (black points), DRI 12 hour integrated sampler results (blue points), and predicted NH_3 mixing ratios predicted from the back trajectory calculations and cattle-only NH_3 emission inventory. Predicted NH_3 is scaled to fit on plot so that NH_3 predicted without deposition (red line) is scaled by a factor of 0.5, while NH_3 predicted with deposition (green line) is scaled by a factor of 2.

9. Figures

Fig 1. Satellite mosiac image showing the Blodgett Forest Research Station in the forested Western foothills of the central Sierra Nevada range of California, and the mixed use (agricultural and urban) areas of the nearby Sacramento Valley area.

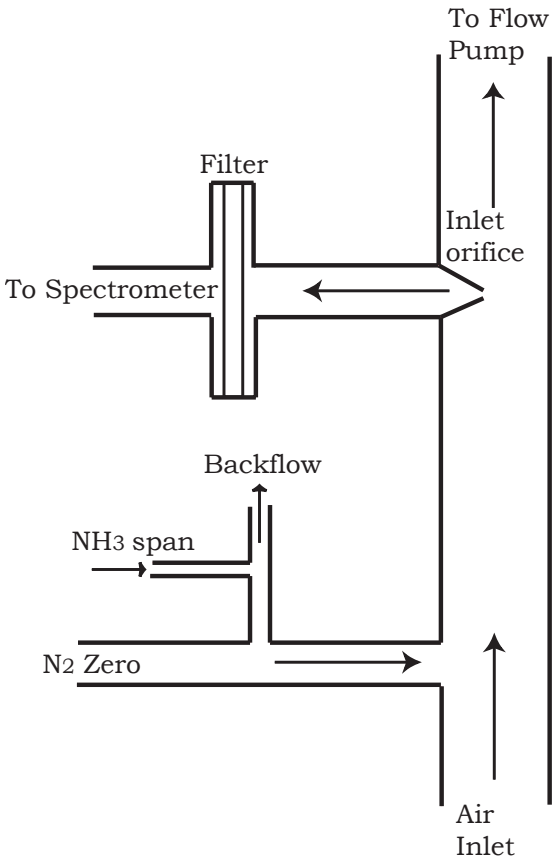

503

504 Fig 2. Schematic illustration of the air sampling manifold with critical orifice flow inlet and

505 air filter. Automated instrument zero and span calibrations are performed by

506 periodically flowing N_2 into inlet, either without or with the addition of NH_3 from a

507 permeation tube source.

508

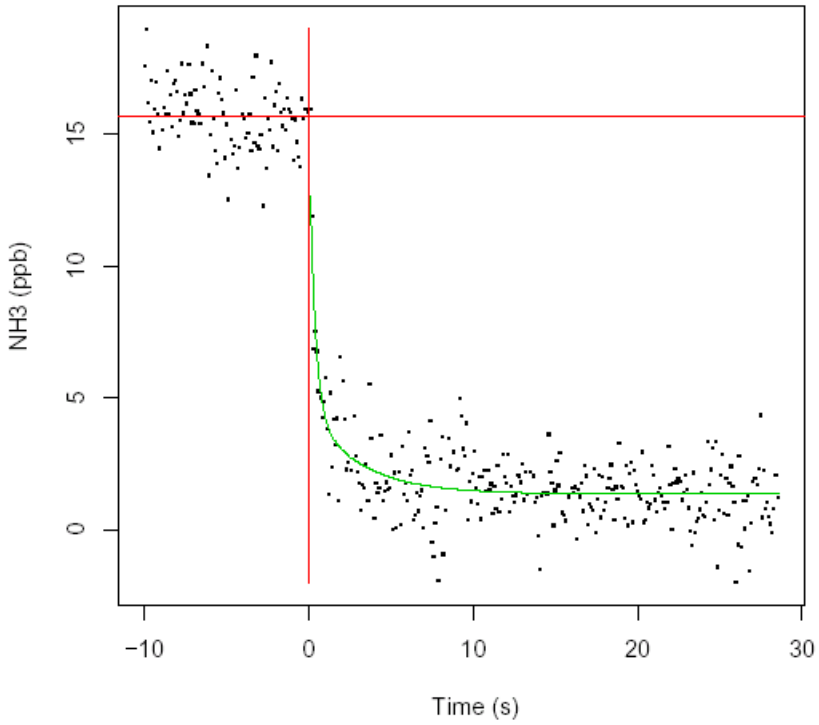

509

510

511 Fig 3. Time series of NH_3 mixing ratio showing transient decay following removal of NH_3 span

512 gas from zero air flow to instrument inlet.

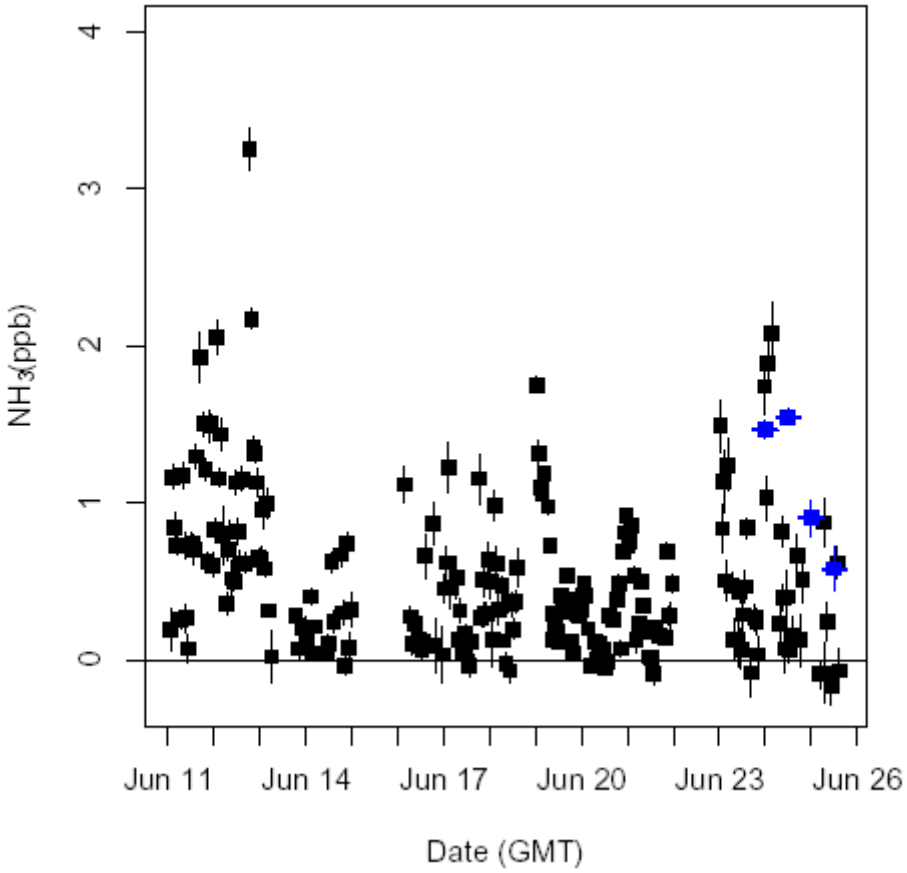

513
514
515

516 Fig 4. Hourly NH_3 mixing ratios measured at Blodgett Forest in June, 2006. NH_3 data from the
517 laser-spectrometer (black symbols) are averaged into 12 hour bins for comparison with
518 integrating filter samples (blue symbols) collected with a sampling system provided by the
519 Desert Research Institute.
520

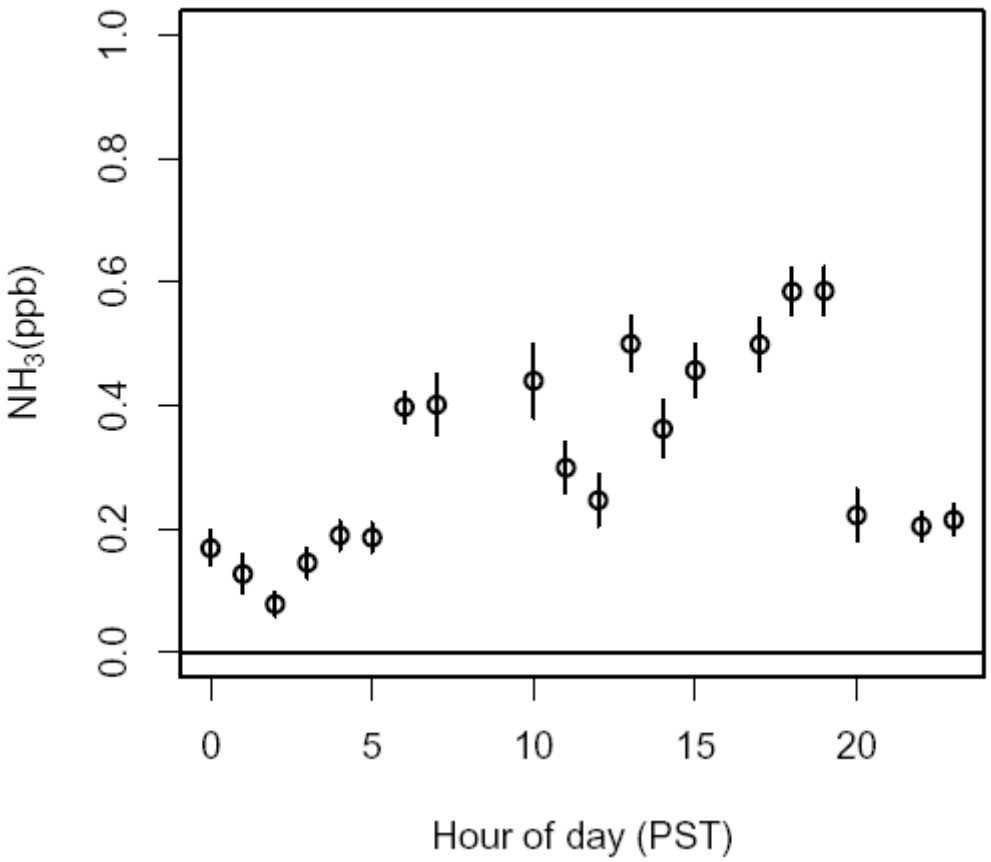

521

522 Fig 5. Mean diurnal variation in surface NH_3 mixing ratio from June 11th to 26th, 2006.

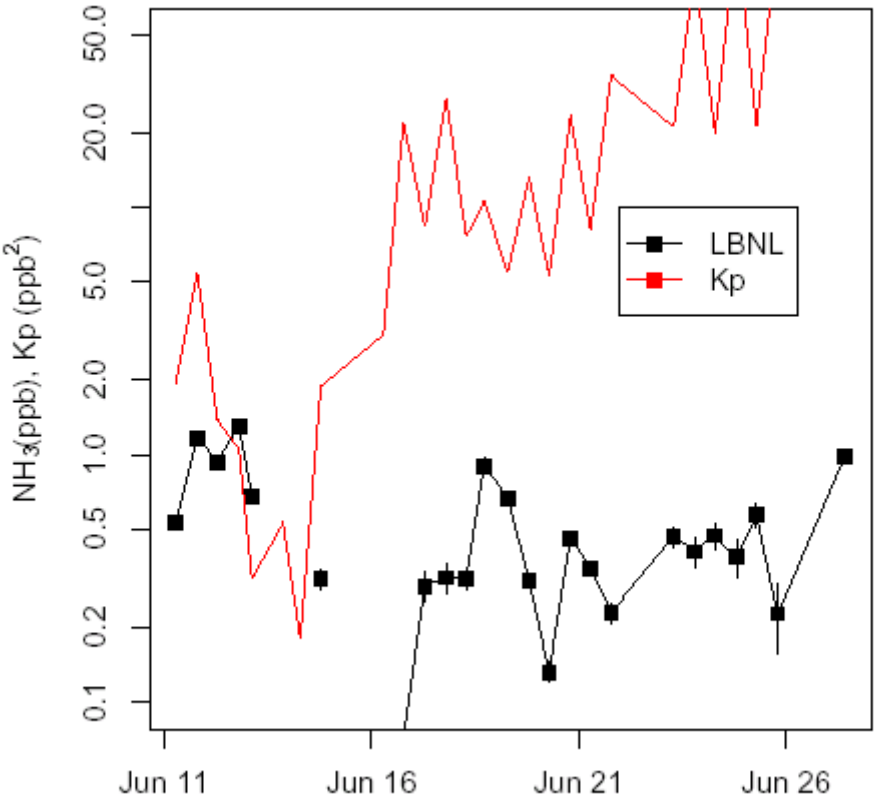

523

524 Fig 6. Comparison of NH_3 mixing ratio (black) and aerosol-gas equilibrium partitioning

525 coefficient, Kp (red), indicating minimum product of gas phase NH_3 and HNO_3 mixing

526 ratios necessary for NH_4NO_3 aerosol to be found in equilibrium with gas phase

527 constituents.

528

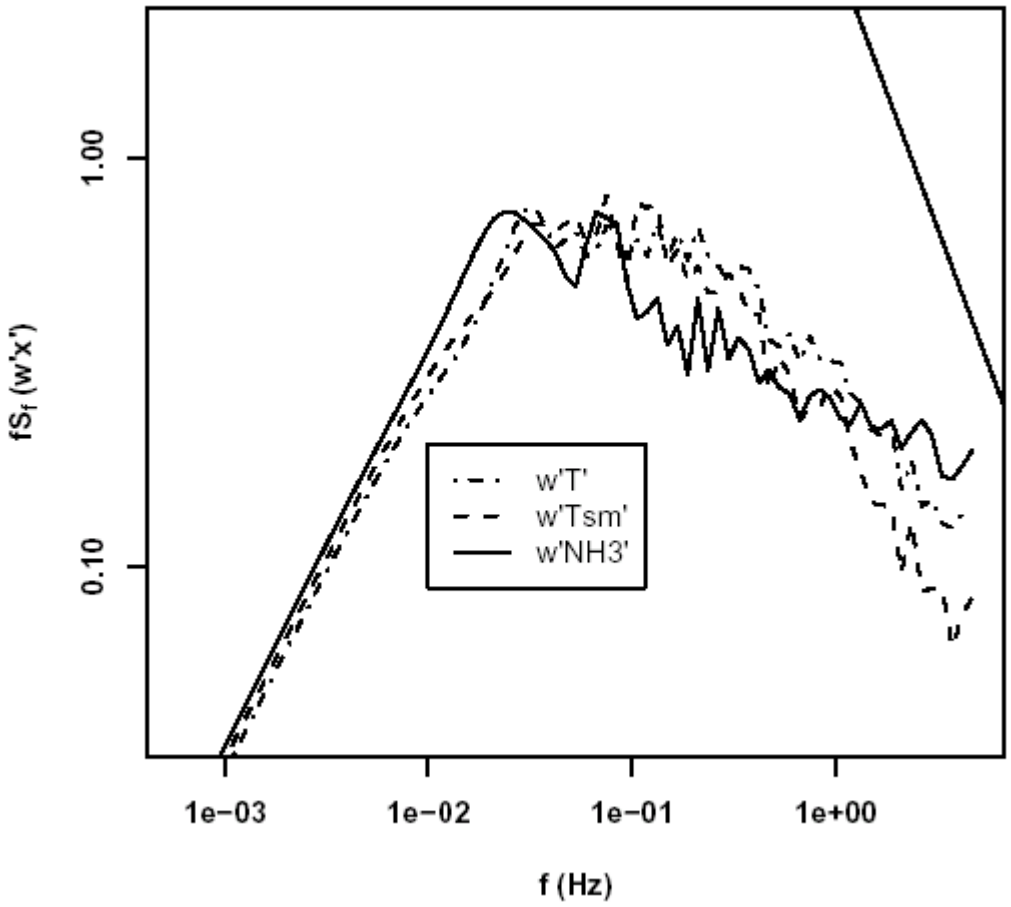

529

530 Figure 7. Power spectra of covariance in vertical wind speed with sonic temperature,

531 w' T' , smoothed sonic temperature, w' T' $_{sm}$, and fluctuations in NH_3 mixing ratio,

532 w' NH_3' . The straight line in upper right shows -4/3 slope expected for fluctuation

533 spectra in an inertial sublayer.

534

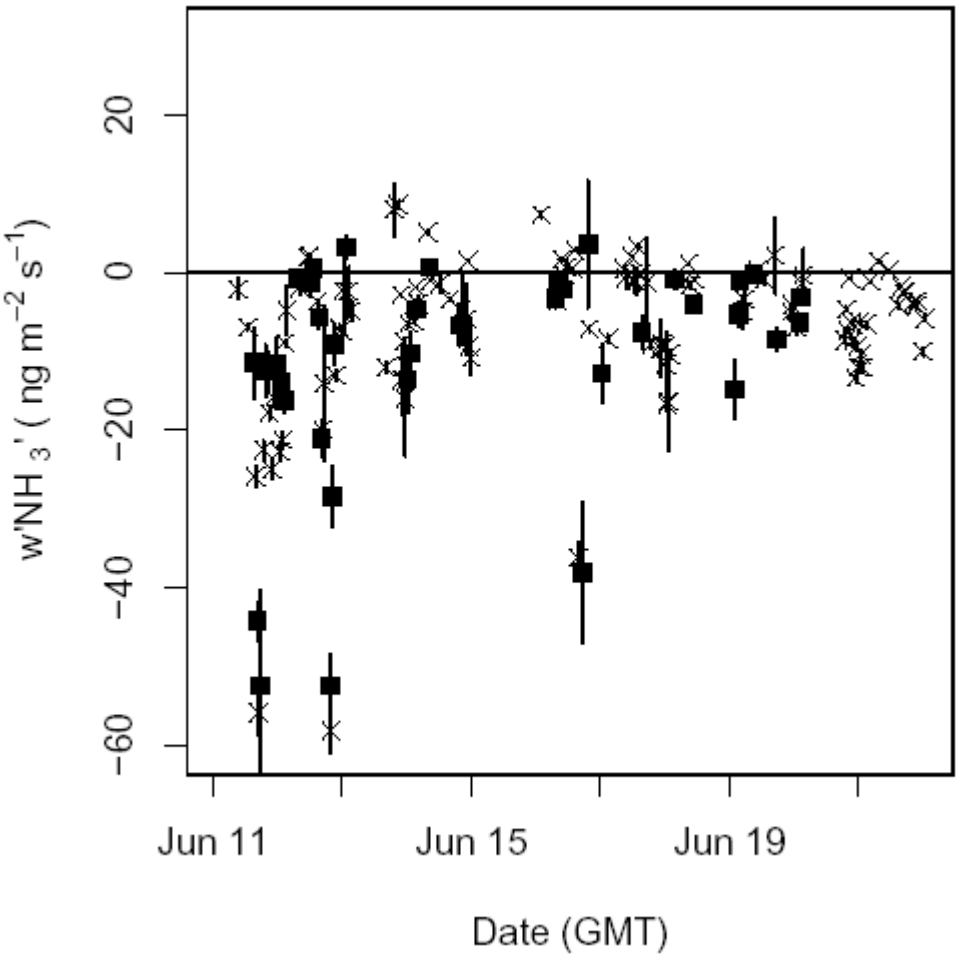

535

536 Figure 8. Eddy covariance measurement of NH_3 flux for all time points (crosses) and for those
537 passing quality control criteria for use in calculating deposition velocities (filled squares).

538

539

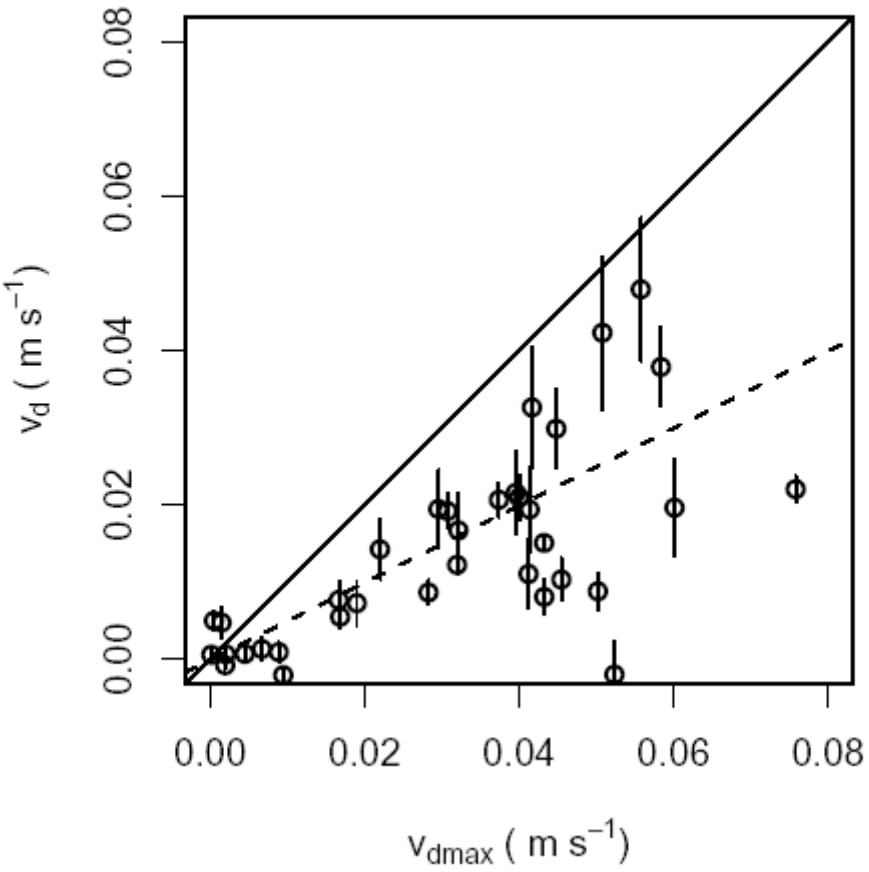

Figure 9. Scatter plot comparison of measured deposition velocity, v_d, and maximum deposition velocity in the case that all molecules reaching the leaf surface are absorbed, v_{dmax}.

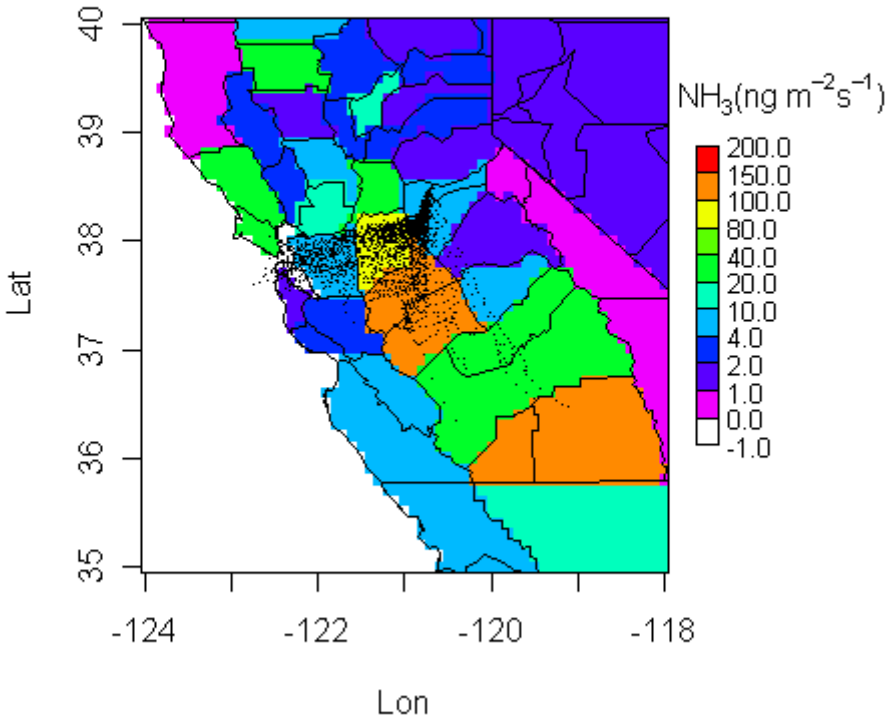

544

545 Figure 10. Map of California showing estimated NH_3 emissions (ng NH_3 m^{-2} s^{-1}) and an
546 example 12hr back trajectory calculation of showing particles converging at BFRS at midday on
547 June 12th, 2006.

548

549

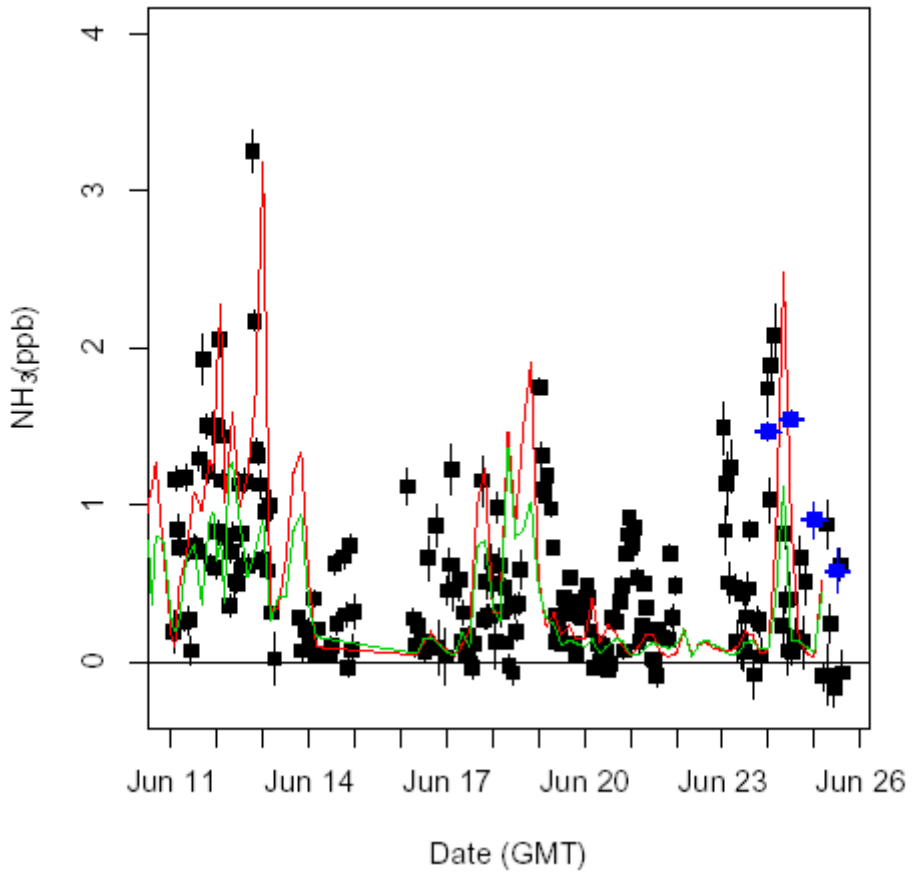

Figure 11. Measured hourly NH_3 mixing ratios from LBNL system (black points), DRI 12 hour integrated sampler results (blue points), and predicted NH_3 mixing ratios predicted from the back trajectory calculations and cattle-only NH_3 emission inventory. Predicted NH_3 is scaled to fit on plot so that NH_3 predicted without deposition (red line) is scaled by a factor of 0.5, while NH_3 predicted with deposition (green line) is scaled by a factor of 2.